Thesis for the Degree of Master of Engineering

Enhanced Efficiency of Polymer Solar Cells and Polymer Light-Emitting Diodes by using a Cathode Interfacial Materials

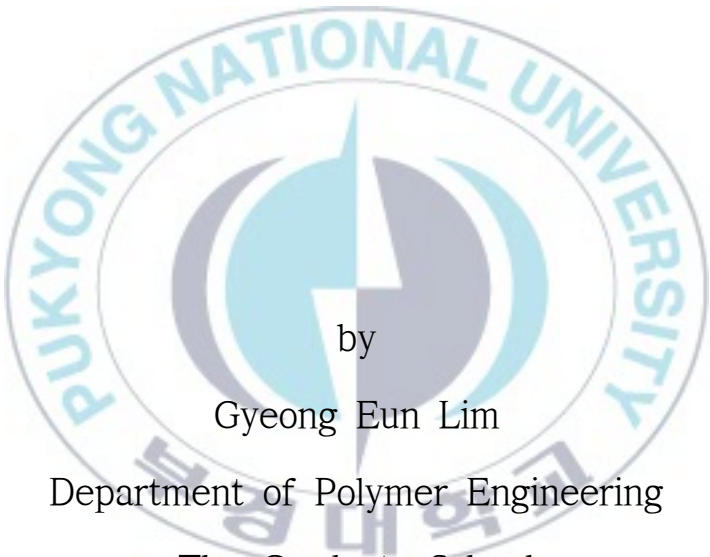

by

Gyeong Eun Lim

Department of Polymer Engineering

The Graduate School

Pukyong National University

February 2015

Enhanced Efficiency of Polymer Solar Cells and Polymer Light-Emitting Diodes by using a Cathode Interfacial Materials
(음극 층간 물질을 사용한 고분자 태양전지와 고분자 발광 소자의 효율 향상)

Advisor : Prof. Joo Hyun Kim

by
Gyeong Eun Lim

A thesis submitted in partial fulfillment of the requirements
For the degree of

Master of Engineering

in Department of Polymer Engineering, The Graduate School,
Pukyong National University

February 2015

Enhanced Efficiency of Polymer Solar Cells and Polymer Light-Emitting Diodes by using a Cathode Interfacial Materials

A dissertation
by
Gyeong Eun Lim

Approved by :

_____
(Chairman) Prof. Seong-Il Yoo

_____
(member) Prof. Mun Ho Kim

_____
(member) Prof. Joo Hyun Kim

February 27, 2015

Contents

List of Figures

List of Tables

음극 층간 물질을 사용한 고분자 태양전지와 고분자 발광 소자의 효율 향상

임경은

부 경 대 학 교 대 학 원 고 분 자 공 학 과

요 약

고분자 태양전지(Polymer solar cells)와 발광소자(Polymer light-emitting diodes)와 같은 유기 광전 소자는 가볍고, 용액공정으로 값 싸고 쉽게 대면적화가 가능하여 차세대 에너지원으로 주목을 받고 있다. 소자 내 전자 수송 능력, 전자 주입능력은 소자의 성능에 영향을 미치는 중요한 요소이며, 이 요소들은 고분자 태양전지에서는 광활성층과 전극 사이에서, 발광소자에서는 발광층과 전극 사이에서의 층간 성질에 따라 크게 달라진다. 층간 성질을 조절하기 위한 방법으로는 층간 물질, 특히 자기조립 단분자막 (self-assembled monolayer (SAM))과 완충층 (buffer layer)이 많이 사용되고 있다. 소자 내에 이와 같은 층간 물질을 적용하였을 때, 영구 쌍극자에 의해 금속의 일함수를 조절하고, 접촉 저항을 줄여 효율을 향상시킨다.

본 연구 에서는 완충층으로 극성을 가진 poly(sodium 4-styrenesulfonate) (PSS-Na) 를 사용하여 고분자 태양전지와 발광소자를 제작하였고, 광전기적 특성과 소자의 계면 특성을 연구하였다.

Chapter I. Introduction

Recently, Organic optoelectronic devices such as polymer solar cells (PSCs) and polymer light-emitting devices (PLEDs) have attracted great attention because they can be applied to a sustainable renewable energy source[1,2]. Organic optoelectronic devices have many advantage that organic materials offer the advantage of cost effective fabrication, as well as the use of large area or flexible substrates. Also, it is possible to modify the chemical structure easily.

Polymer solar cells (PSCs) have the advantage of being less expensive and solution processible by spin coating, spray coating and roll-to-roll type processing techniques. The most widely studied polymer blend system is based on a solution processed p-type poly(3-hexyl-thiophene) (P3HT) polymer and an n-type [6,6]-phenyl C61 butyric acid methyl ester (PCBM) fullerene. This polymer blend system has led to efficiencies as high as 5%[3]. Efficiencies as high as 6 to 7% have been achieved with polymer:fullerene bulk heterojunction (BHJ) systems by developing lower band-gap polymer materials that can absorb a broader range of the solar spectrum[5,6].

Polymer light-emitting diodes (PLEDs) have attracted great due to their high brightness, fast response, large viewing angle, simple manufacture process and flexibility. Typical multilayered PLEDs consist of a transparent anode (i.e. an indium tin oxide (ITO) coated glass substrate), a hole transport material (HTM), a

light emitting layer and electron transport material, and a metallic cathode.

Significant efforts over the past decades have been made to improve the efficiency of polymer-based optoelectronic devices using a variety of processing strategies [7-19]. These approaches have included a better understanding of the device physics,[7] new materials for high performance[8-13], optimization of the morphologies by advanced processing methods[14-16], and advanced device architectures[17-19]. Among them, the interfacial engineering is one of the important strategies. In other words, the charge transporting properties are important factors for influencing the performances of the devices. This is strongly related to the interfacial properties between the active layer and the cathode or the anode. Insertion of a buffer layer at the interfaces was used to optimize the properties between the semiconducting layer and both the electrodes. A thin layer of PEDOT:PSS[20], self-assembled monolayer (SAM) modification[21-23], or metal oxides such as WO_3 and MoO_3 were mostly used for improving the hole transporting properties between the active layer and the anode. And the materials of buffer layer reported in PSCs include alkali-metal compound such as LiF, metal oxides, TiO_x, water or alcohol soluble conjugated polymer electrolytes (CPEs) [24-27], cationic conjugated polymer electrolytes with quaternary ammonium salt[28-31], non-conjugated polymer electrolytes based on viologen derivatives[32,33], anionic conjugated polymer electrolytes[34,35] with sulfonate and non-conjugated cationic polyelectrolytes[32,33].

Chapter I-1. Structure and basic principle of Devices

I-1-1. Conventional polymer solar cells (CPSCs)

Conventional Polymer solar cells (CPSCs) architecture (Figure.1-1) consists of a transparent conducting metal oxide coated with a poly(3,4-ethylenedioxythiophene):poly(styrenesulfonate) (PEDOT:PSS) hole-transporting layer followed by the active BHJ layer. To complete the device, a low work function metal electrode (Al, Ca/Al) is evaporated on top as an electron-collecting electrode [36].

Polymer solar cells follow the four steps and processes to obtain Power Conversion Efficiency (PCE). (Figure.1-2) The first is absorption of light normally by a semiconductor, this will generate an exciton, or a hole and electron pair bound together by a weak binding energy. Next the exciton will diffuse around the material until it reaches a region were the third step, charge separation or quenching can occur, this will normally be at the donor acceptor (DA) interface. In quenching the electron and the hole are fully separated from each other as the electron will enter a lower energy state in the acceptor material. From here the hole and electron must travel to their respective electrodes in what is called charge transport .

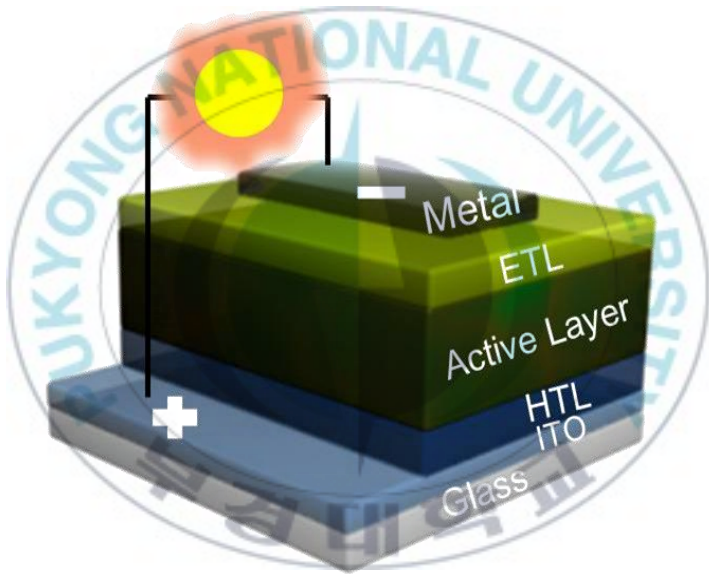

Figure I-1. Typical structure of CPSC.

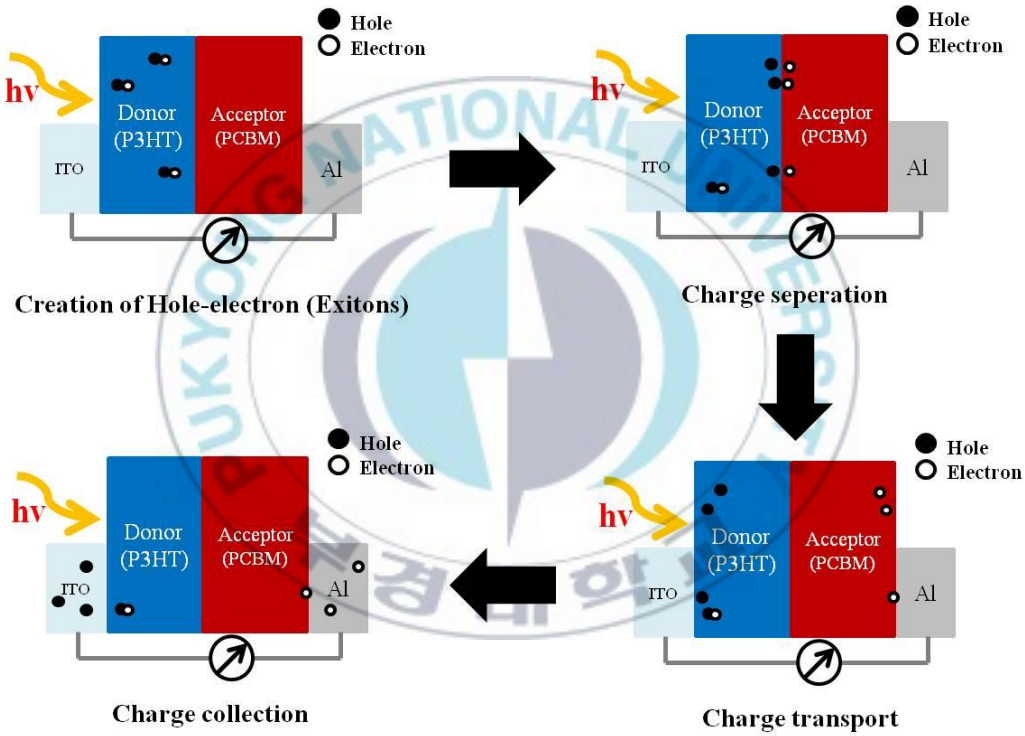

Figure II-2. Operating mechanism of PSC.

I-1-2. Inverted polymer solar cells (IPSCs)

The name “inverted” describes the reversed change in polarity of solar cell. In case of CPSCs, the device structure is ITO/PEDOT:PSS/P3HT:PCBM/Al, ITO and Al electrodes collect holes and electrons, respectively. In case of IPSCs, ITOs collect electrons and metal electrodes collect holes. Higher work function metal electrodes like gold (Au), silver (Ag), and copper (Cu) are generally used as top metal electrodes in inverted solar cell architecture [37-40]. These metal electrodes are air-stable and make good contact with organic layers. Metal oxides such as ZnO[41,42], TiO_x[43-45] is used as electron transporting layer, eliminating the problem of the acidic PEDOT:PSS on ITO. The process of the generation of current is same with CPSCs.

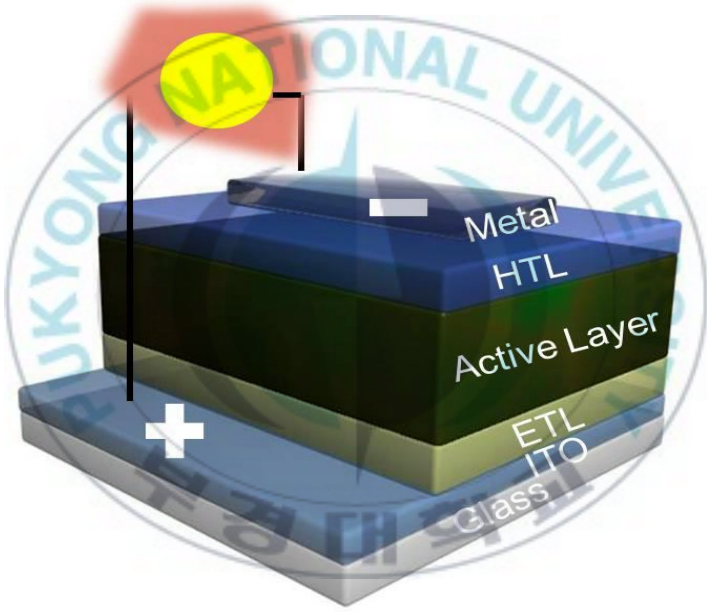

Figure I-3. Typical structure of IPSC.

I-1-3. Polymer light-emitting diodes (PLEDs)

A PLED is a thin-film solid state device, which makes it easier to apply to flexible displays because of its simple fabrication process and reduced distortion according to the geometric form of display. The structure of PLEDs is showed in the Figure 1-3. (ITO/HTL/Emissive Layer (EML)/ETL/cathode)[46].

When the voltage is applied across the device, these organic thin films emit light. This light emission is based upon a luminescence phenomenon wherein electrons and holes are injected and migrate from the contacts toward the EML. When these carriers meet, they form excitons (electron-hole pairs) that recombine to emit light of a certain wavelength (e.g., red, green or blue) according to the specific organic materials employed[47].

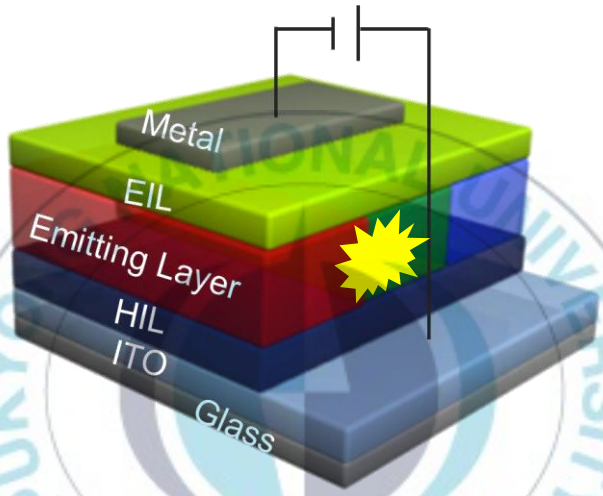

Figure I-4. Typical structure of PLEDs.

I-2. Parameters of Devices

I-2-1. Parameters of polymer solar cells

The main parameters of solar cells are the short-circuit current density (J_{sc}) , the open-circuit voltage (V_{oc}) and the fill factor (FF) from the illuminated J-V characteristic as illustrated in Figure 1-5. The V_{oc} is the voltage for which the current in the external circuit equals zero. At the donor-accepter interface generate ΔE between the HOMO energy level of donor and the LUMO energy level of acceptor which is the energy difference. The J_{sc} is the current through the solar cell when the voltage across the solar cell is zero[48]. And the J_{sc} is due to the generation and collection of light-generated carriers.

The fill factor is the ratio between the maximum power ($P_{max} = J_{mp} \times V_{mp}$) generated by a solar cell and the product of the V_{oc} and the J_{sc}.

$$FF = \frac{J_{mp}}{J_{sc}} \frac{V_{mp}}{V_{oc}}$$

And, the FF is a measure of the "squareness" of the IV curve, a solar cell with a higher voltage has a larger possible the FF since the "rounded" portion of the IV curve takes up less area.

The power conversion efficiency (PCE) is calculated as the ratio between the generated maximum power and the incident power under AM 1.5 conditions.

$$PCE = \frac{J_{sc} V_{oc} FF}{P_{in}}$$

P_{in} is the incident light power which is standardized as 100 mW/cm^2.

IPCE (incident photon to electron conversion efficiency) is a measure of the photon to electron conversion efficiency at a particular irradiation wavelength.

$$\text{IPCE (Incident Photon to electon Conversion Efficiency)}(\%) = \frac{\text{Number of emitted photons from a solar cell}}{\text{Number of incident photons to a solar cell}} \times 100$$

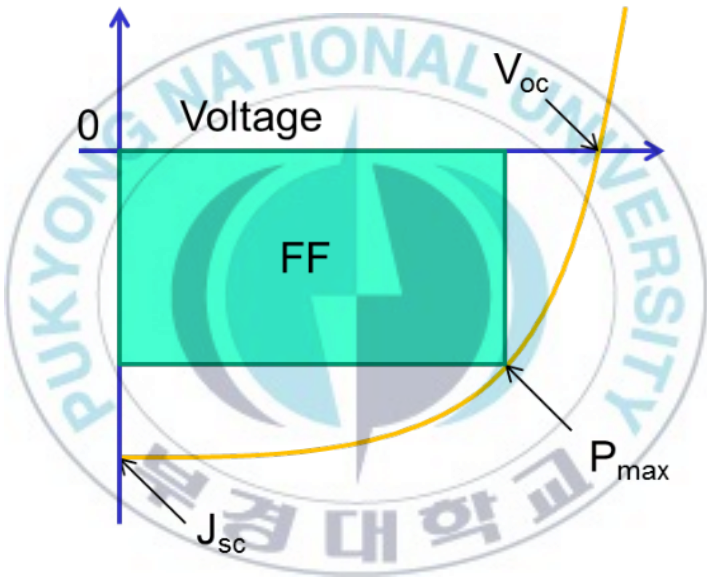

Figure I-5. J-V characteristics of polymer solar cells.

I-2-2. Parameters of polymer solar cells (resistance)

There are another parameters which affect to the PCE. One is the series resistance (R_s), the other is the shunt resistance (R_{sh}). Their interaction determines how the current flows in the device[49]. The series resistance (R_s) is one of the key parameters affecting the performance of organic photovoltaic devices. The main impact of series resistance is to reduce the fill factor, although excessively high values may also reduce the short-circuit current. Usually R_s is estimated from the current–voltage J–V curve slope at large forward voltage. The processes contributing to R_s are voltage-dependent through physical mechanisms originated at different layers or interfaces within the device. Interfaces between the active layer blend and interfacial layers or metallic contacts may well add more resistance in series because of partial energy level alignment which affects optimal interface charge transfer. Finally charge carrier transport within the active layer itself could also be a source for incrementing the series resistance [50-52].

The R_{sh} denotes the current losses in the cells, such as the current leakage from the edge of the cell. Ideal R_{sh} should approach infinity, so current flows through R_{sh} is zero, in other words there is no current leakage in the device. If the R_{sh} is small, the current flowing through it cannot be neglected. Moreover, the current will change with the applied voltage, which makes the J–V curve deviate from ‘‘square’’ and thus lead to a lower FF.

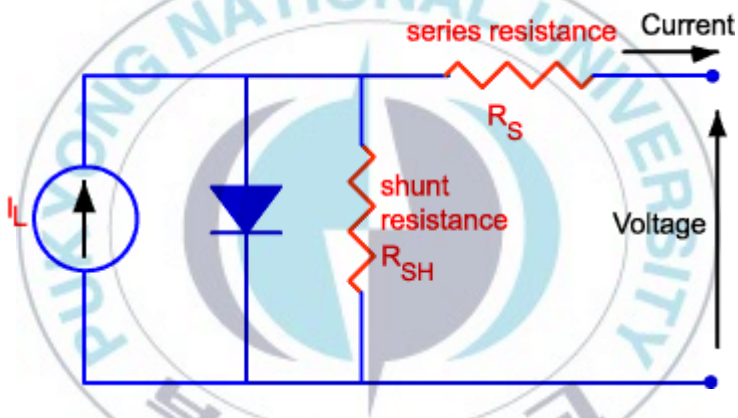

Figure I-6. Series and shunt resistances in a solar cell

I-2-1. Parameters of polymer light-emitting diodes

The efficiency of an PLED is characterized by its quantum efficiency, the current efficiency in cd A^{-1} (η_P) or the luminous efficiency (η_P) in lm W^{-1}. The current efficiency (η_P), expressed in cd A^{-1}, is another way to characterize the quality of a device and represents the ratio of the luminance (L) to the current density (J) flowing into the diode. The luminous efficiency (η_P) expressed in lm W^{-1} is the ratio of the optical flux to the electrical input and is given by:

$$\eta_P = \frac{L\pi}{J V} = \eta_L \frac{\pi}{V}$$

where V is the working voltage.

A very basic and yet very simple measurement for PLEDs are current density – voltage (J-V) characteristics as it directly shows if the device is working properly and gives a first impression on its quality. A bias voltage sweep is applied to the device and its current response is recorded. Furthermore, the intensity of the generated light can be recorded simultaneously, the light intensity correlates to the luminance L. The corresponding measurement is called current density – voltage – luminance (J-V-L) characteristics[53].

I-3. Interfacial layer

I-3-1. Function of interfacial layer

The interfacial layer which is coated between the active layer (or Emissive layer) and the electrodes is vital for extremely efficient and stable devices. There are several functions of interfacial layer.[54] The first is to control the barrier height between active layer and the electrodes. The understanding of the function of those interfacial layers and the resulting band alignment (between metal and organic layer) is essential for the proper choice of such interfacial materials. Second is to determine the polarity of the device. Third is to prohibit a chemical or physical reaction between the polymer and electrode. The protection of the active layer from oxygen and water of the atmosphere by and interfacial layer. And last thing is to act as optical spacer. An optical spacer layer can help to improve the short-circuit current of PSC device. The optical spacer redistributes the maximum light intensity to be within the charge-separating BHJ layer[55].

I-3-2. Materials of interfacial layer

I-3-2-1. PEDOT:PSS

PEDOT:PSS, poly(3,4-ethylenedioxythiophene) doped with poly(styrenesulfonate), is a stable, water soluble conjugated polymer which is used as a hole transporting layer in organic optoelectronic devices. The main functions of PEDOT:PSS is to improve selectivity of the anode, of the electrode/active layer contact, on account of the higher work function relative, increase photovoltage through the surface enrichment of PSS components. Furthermore, it can be used to match the highest occupied molecular orbital (HOMO) of the donor. The reason why PEDOT:PSS is widely used as p-type interfacial layer. The chemical structures of PEDOT and PSS are depicted in Figure I-7.

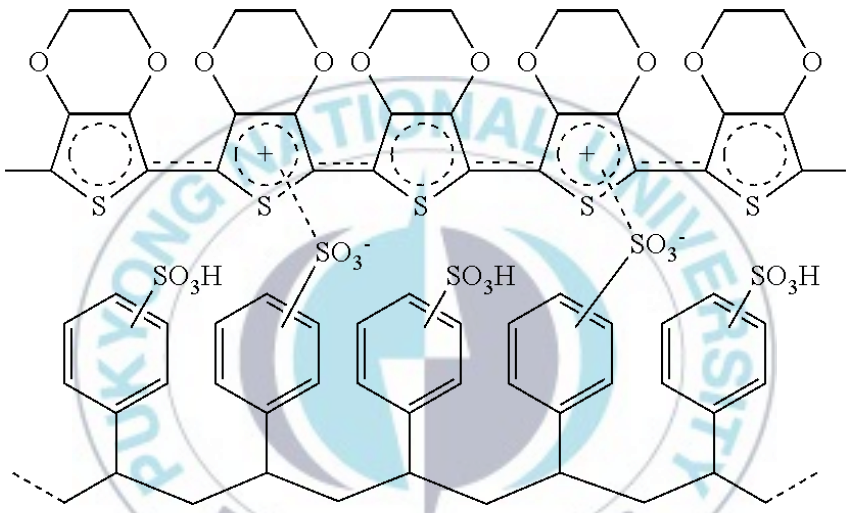

Figure I-7 Structure of PEDOT:PSS

I-3-2-2. Alkali-metal compounds (LiF)

Lithium fluoride (LiF) is promising electron extraction materials for PSCs. By adding the lithium Fluoride interlayer it will increase device lifetime and prevents the formation of trap state due to oxidation of the metal aluminum interface. Dissociation of the LiF and subsequent chemical reaction (doping) of the organic layer Formation of a dipole layer leading to a vacuum level offset between the organic layer and the Al Protection of the organic layer from the hot Al atoms during thermal deposition. Insertion of thin layer Lithium Fluoride less than 15 Angstroms increases the fill factor of the organic solar cell device. The increased of the fill factor is due to the formation of buffer layer Ohmic contact. Several mechanisms have been suggested thus far, including Lowering of the effective work function of the aluminum[56-59].

I-3-2-3. Metal oxide (TiO_x**)**

The TiO_x layer allows the flow of electrons and blocks transport of holes. TiO_x is postulated to block the passage of oxygen and humidity into the active layer. When a TiO_x thin film is inserted into the device structure, the lifetimes of organic solar cells and PLEDs are improved by approximately two orders of magnitude. The results described here focus on TiO_x as a passivation layer on organic FETs. The TiO_x layer contains both Ti-OR(OR¼ alkoxide) functionalities and Ti-OH groups. The Ti-OR functionalities are photooxidized, consuming O_2 and generatingCO_2, H_2O gas products and [HCOO-] and Ti-OH moieties. This photo-chemical reaction forms the basis for TiO_x films to remove oxygen when exposed to ultraviolet light[60-62].

I-3-2-4. Self-assembled monolayers (SAMs)

SAMs (Self-assembled monolayers) are organized layers of molecules which spontaneously forms on a solid surface. SAMs are easily modified at a single molecular level as well as at the assembled levels. Self-assembly of organic molecules is a useful method for modifying systematically the chemical properties of solid surfaces in order to control their functions in such processes as wetting, adhesion, friction. Also SAMs offer a unique combination of physical properties that allow fundamental studies of interfacial chemistry, solvent-molecule interactions and self-organization. Their well-ordered arrays and ease of functionalization make them ideal model systems in many fields[63,64].

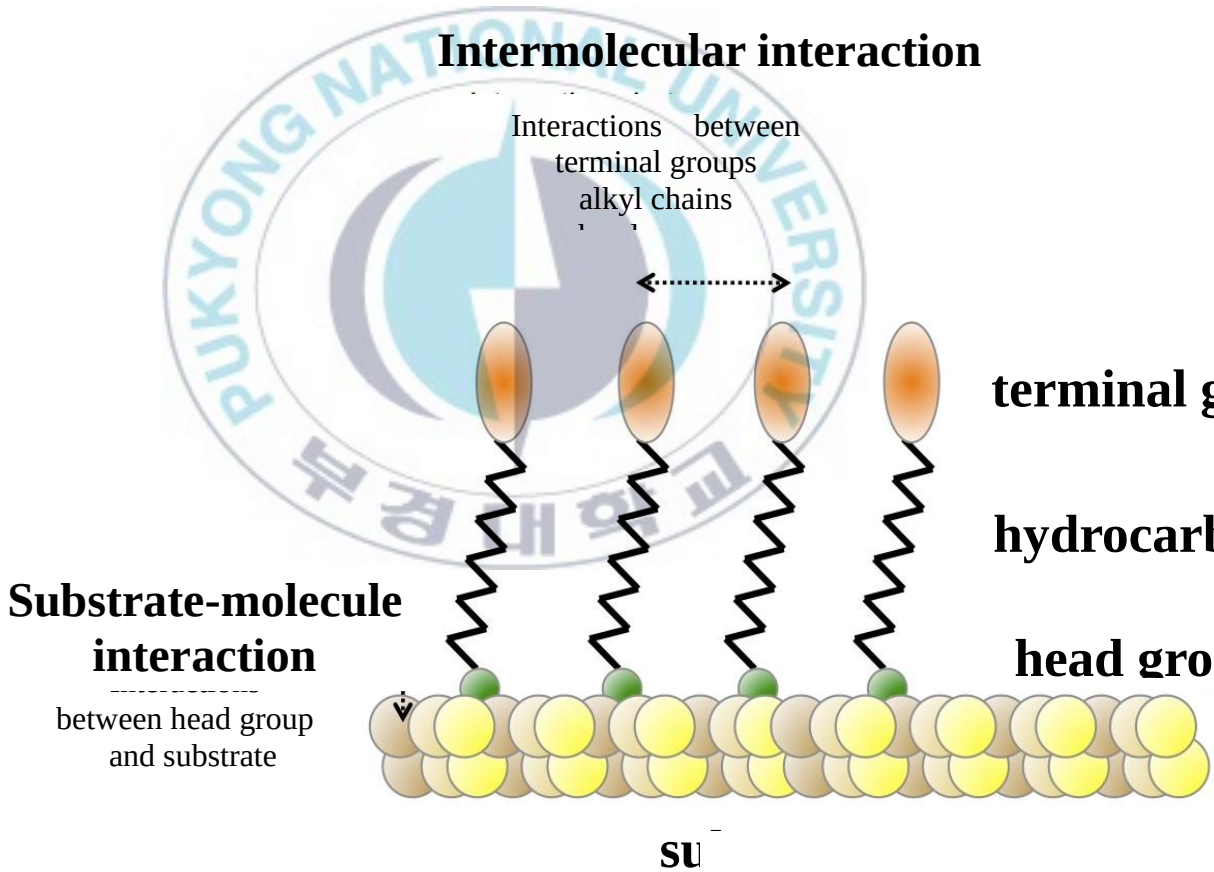

FigureI-8. The structure of self-assembled monolayers (SAMs)

I-3-2-5. Conjugated polyelectrolytes (CPEs)

Conjugated polyelectrolytes (CPEs) are defined as polymers having backbones with π-delocalized electronic structures and pendant substituents with ionic functionalities. In particular, the π-conjugated backbone have many functions, including strong optical absorption and fluorescence, conductivity for neutral (exciton) and charged (polaron) states, and an amplified response to external stimuli owing to the delocalized electronic structure of the backbone. In addition, the polyelectrolyte functionality imparts the materials with the properties intrinsic to polymer electrolytes, namely, water solubility, ionic conductivity, strong intra- and interchain interactions, interaction with ions in solution, surface activity, and a propensity to adsorb at interfaces.[65,66]

I-3-2-6. Non-conjugated polyelectrolytes (nCPEs)

Non-conjugated polyelectrolytes (nCPEs) equipped with charged ionic groups in their chemical structure may be ideal interfacial materials. Although polymer have backbones without π-delocalized electronic structures, NCPEs also have many functions. The main function of NCPEs are to increase the built-in-potential by inserting NCPEs interfacial layer, to improve charge transportation because of the existence of interface dipole and reduce recombination loss due to the increase in built-in field and charge carrier mobility. Few studies on using NCPEs as a cathode interfacial layers have been reported. In case of poly(ethylene oxide) (PEO), the V_{oc} was dramatically enhanced by up to 200 mV, and a noticeable enhancement of the FF and the J_{sc} were observed as well, resulting in the enhancement of the PCE by 50%. Because the built-in potential was increased upon inserting the PEO interfacial layer and thus improving charge transportation. Poly(vinyl alcohol) (PVA) was used in polymer solar cells and polymer light-emitting diodes as cathode interfacial layer. The best PCE of PSC with the PVA film as a cathode interfacial layer is 3.27%, which is a 27% increase compared to that of PSC without the PVA film (2.58%). The PCE improvement is due to enhancement of the short circuit current, the fill factor, and the open circuit voltage, simultaneously. Improvement of the performances of the devices is due to the fact that the PVA film reduces a Schottky barrier by the formation of favorable interface dipoles and improves the interface properties. And Yang et al.

reported the application of poly(vinylpyrrolidone) (PVP) as a cathode interfacial layer in PSCs. For the case of incorporation of PVP by spin coating, the PCE of the device (3.90%) is enhanced by 29%, suggesting the increase of the charge collection upon the incorporation of a PVP as a cathode interfacial layer.

I-4. Measurement

The thickness of the film was measured by an Alpha-Step IQ surface profiler (KLA-Tencor Co.). The work function measurements were carried out using a UPS (VG Scientific Co.) with a He I source (hν= 21.2 eV) at a pressure of 1 x 10^{-8} Torr. A -3 V was applied to a sample during the measurements to distinguish between the analyzer and sample cut-off. The surface energy (γ) of the active layer with or without interfacial layer was evaluated by the measurements of the static advancing contact angle with deionized water and diiodomethane. The contact angles (KRUSS, Model DSA 100) were entered in the Wu model (harmonic mean) for the calculation of the dispersive and polar components of the surface energy. The effective work function was obtained by Kelvin probe (KP) measurements (McAllister Technical Services, KP 6500) of the contact potential difference between the sample and the KP tip. The KP tip work function was 5.203 ± 0.011 eV. The AFM topography images were taken using a Digital Instruments (Multi Mode SPM) operated in the tapping mode. The current density−voltage measurements under 1.0 sun (100 mW/cm^2) condition from a 150 W Xe lamp with a 1.5 G filter were performed using a KEITHLEY model 2400 source measure unit. A calibrated Si reference cell with a KG5 filter certified by the National Institute of Advanced Industrial Science and Technology was used to confirm 1.0 sun condition. The incident photon to collected electron efficiency (IPCE), external quantum efficiency, was calculated by

$$\text{IPCE}\ (\%) = 1240 \times J_{sc} / \left(\frac{\lambda}{I_p}\right)$$

where J_{sc} (μA/cm^2) is the short circuit current density measured at the wavelength λ (nm) and I_p (W/m^2).

Chapter II. Non-conjugated Poly(sodium 4-styrenesulfonate) as an Interlayer for Applications in Polymer Solar Cells and Polymer Light Emitting Diodes

II-1.Introduction

Optoelectronic devices such as polymer light-emitting diodes (PLEDs) and polymer solar cells (PSCs) have been receiving great attention in recent years, because it has many advantages including light weight, low fabrication cost, and the possibility of their application properties. light weight, easy large-area fabrication, and low fabrication cost by the solution process. The charge transporting and injecting/collecting properties are critical factors for influencing on the performances of the devices. These are related to the interfacial properties between the emissive layer (or the active layer) and the electrodes. In particular a cathode buffer layer, which is applied between the emissive layer (or the active layer) and cathode, has been studied to improve the metal electrode efficiency in injecting and collecting negative carriers[67].

Recently, few studies on using non-conjugated cationic and anionic polymers such as a poly(ethylene oxide) (PEO), poly(4-vinyl pyrrolidone) (PVP) and poly(vinylalcohol) (PVA)[68] have been demonstrated for a cathode buffer layer. The efficiency of the devices with these materials as a cathode buffer layer was dramatically improved by the formation of favorable interface dipole which

reduces the work function of metal as well as the electrical contact resistance. Therefore, a non-conjugeted anionic polymer such as poly(sodium 4-styrenesulfonate) (PSS-Na) might be used as a cathode buffer layer. PSS-Na is well known commercially available non-conjugated anionic polyelectrolyte and very good soluble in polar protic solvents such as water or mixture of water and alcohol. The solubility of PSS-Na in polar protic solvents offers the options available for the utilization of a buffer layer in the optoelectronic devices. We investigated the effect of PSS-Na as buffer layer in PLEDs and PSCs.

II-2. Experiment Section

II-2-1. Materials

Chemicals were purchased from Aldrich Chemical Co. and Alfa Aesar and were used as received unless otherwise described. Poly(sodium 4-styrenesulfonate) (Cat. No. 45851, Mw = 75000 g/mol) and poly(4-styrenesulfonic acid) was purchased from Alfa Aesar. Regioregular P3HT (Cat. No. 4002-EE) and PCBM (Cat No. nano-cPCBM-BF) were purchased from Rieke Metals Inc. and nano-C, Inc., respectively. PF9B was used as an EML and synthesized according to the literature procedures [69].

II-2-2. Fabrication of PSCs

For fabrication of PSCs with a structure of ITO/PEDOT/active layer (P3HT:PCBM)/PSS-Na/Al, a thickness of 40 nm of PEDOT:PSS (Baytron P, diluted with 2-propanol 1:2 v/v) was spin-coated on pre-cleaned indium tin oxide (ITO) glass substrate (sheet resistance = 15 ohm/sq). After being baked at 150 ^{o}C for 10 min under the air of a PEDOT:PSS layer, the Active layer was spin-cast from the blend solution of P3HT and PCBM (20 mg of P3HT and 20 mg of PCBM dissolve in 1 mL of *o*-dichlorobenzene (ODCB)) at 600 rpm for 40 s and then dried in covered petri dish for 1 hour. Prior to spin coating, the photoactive solution was filtered through a 0.45 μm membrane filter. The typical thickness of the active layer was 200 nm. Before cathode deposition, buffer layer of PSS-Na prepared by spin coating with different concentration of solution of PSS-Na at 4000 rpm for 60 s. The typical thickness of a PSS-Na film was less than 5 nm. The thickness of PSS-Na layer was controlled by the concentration of PSS-Na solution. The Al layer was deposited with a thickness of 100 nm through a shadow mask with a device area of 0.13 cm^2 at 2 x 10^{-6} Torr. After the cathode deposition, the device was thermally annealed at 150 ^{o}C for 20 min in the glove box (N_2 atmosphere).

Ⅱ-2-3. Fabrication of PLEDs

For fabrication of PLEDs with a structure of ITO/PEDOT/EML (PF9B)/PSS-Na/Al, a thickness of 40 nm of PEDOT:PSS (Baytron P, diluted with 2-propanol 1:2 v/v) was spin-coated on pre-cleaned indium tin oxide (ITO) glass substrate (sheet resistance = 15 ohm/sq). After being baked at 150 ^{o}C for 10 min under the air, an emissive polymer solution (10 mg/mL in toluene) was spin coated on to PEDOT:PSS layer at 2000 rpm for 60 s. Prior to spin coating, the emissive polymer solution was filtered through a 0.45 μm membrane filter. The typical thickness of the EML was 60 nm. Before cathode deposition, IFL of PSS-Na prepared by spin coating with different concentration of solution of PSS-Na at 4000 rpm for 60 s. The typical thickness of a PSS-Na film was less than 5 nm. The thickness of PSS-Na layer was controlled by the concentration of PSS-Na solution. The Al layer was deposited with a thickness of 100 nm through a shadow mask with a device area of 0.13 cm^2 at 2 x 10^{-6} Torr.

Ⅱ-3. Results and Discussion

Ⅱ-3-1. Characterization of PSCs and PLEDs with PSS-Na

To confirm the effect of the interfacial dipole between active layer and metal surface, we measured by ultra photoelectron spectrometer (UPS) to know the effective work function of the Al and the PSS-Na coated Al.[70] PSS-Na has sodium sulfate salt on the side chain, which is a very polar and has permanent dipole. Therefore, as shown Figure II-1, the work function of the PSS-Na coated Al and the Al is 4.22 and 4.32 eV, respectively. In order to check the work function variation by the PSS-Na thin film, we performed the measurements of the work function by the Kelvin probe microscopy (KPM). The effective work function of a thin layer PSS-Na coated Al obtained from the KPM was 4.16 ± 0.03 eV, which is smaller than the effective work function of PSS-Na coated Al (4.30 ± 0.02 eV). The work function of a thin layer of PSS-Na coated Al was smaller than that of Al. These results support that the work function of the Al cathode is reduced by the formation of interface dipole. From this result, the reduction of Schottky barrier was small and the efficient transporting/injecting of electrons is expected in PSCs and PLEDs. The electron injection properties are enhanced by PSS-Na between the emissive layer and the cathode.

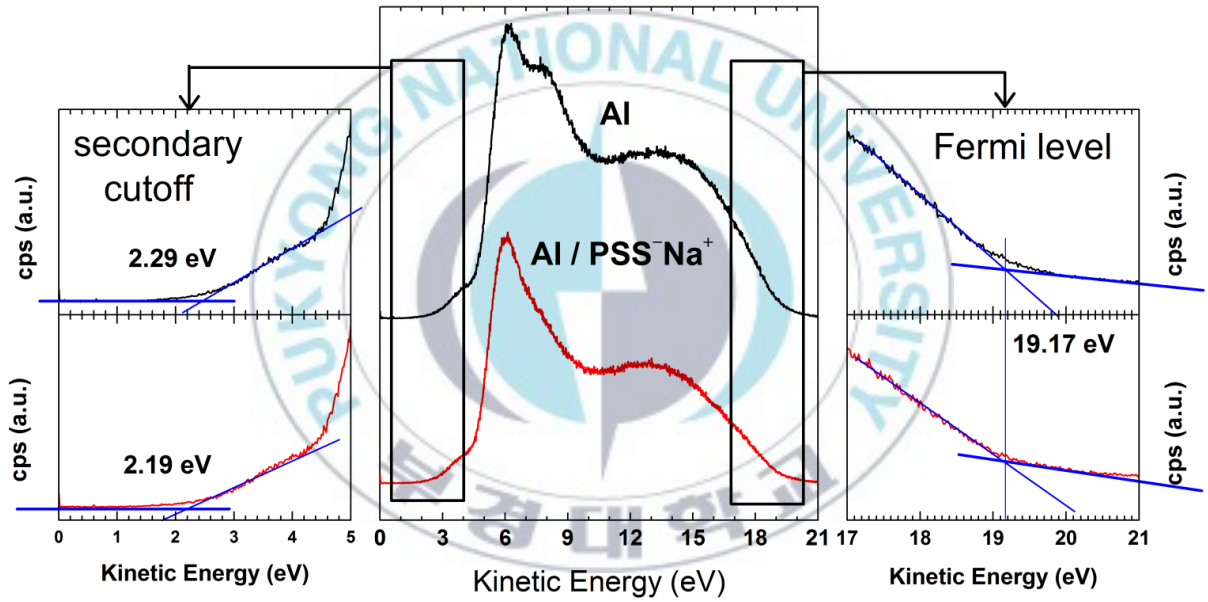

Figure II-1. UPS spectra of Al and PSS-Na treated Al

Ⅱ-3-2. Photovoltaic properties of PSCs

Conventional type PSCs with a structure of ITO/PEDOT:PSS (40 nm)/P3HT:PCBM (1:1by$_{wt.}$)(200 nm)/PSS-Na (5 nm)or without PSS-Na/Al (110 nm) are fabricated to investigate the characteristics of PSS-Na as a buffer layer. PSS-Na dissolved in methanol/water mixture with a concentration of 0.1 mg/mL, 0.5 mg/mL, 1.0 mg/mL was spin-coated onto the P3HT:PCBM active layer to investigate the effect of PSS-Na layer. Fig.II-3 shows current density-voltage curves of PSCs under AM1.5G simulated illumination with an intensity of 100mW/cm^2, and the photovoltaic parameters are summarized in Table 2-1. As shown in Table 2-1, the V_{oc} value of all the devices with the PSS-Na film were 0.61 V, the V_{oc} of the reference device were 0.59 V. The V_{oc} value of the devices were slightly higher than the V_{oc} of the reference device. Our results presumably due to that the reduction of Schottky barrier is quite small. Therefore, the effective work function of Al/PSS-Na shows smaller than Al (without PSS-Na). As seen in Table 2-1, Short-circuit current (J_{sc}) value of devices are -7.64 mA/cm^2 (without PSS-Na), -8.25 mA/cm^2, (PSS-Na 0.1 mg/mL), -8.43 mA/cm^2 (PSS-Na 0.5 mg/mL), -7.47 mA/cm^2 (PSS-Na 1.0 mg/mL), respectively. The fill factor (FF) value of the device with concentration of 0.1 mg/mL, 0.5 mg/mL and 1.0 mg/mL PSS-Na in H_2O/MeOH are 53.5%, 54.9% and 54.7%. The best power conversion efficiency (PCE) of the device with concentration of 0.5 mg/mL PSS-Na in

H_2O/MeOH was 2.82%, which is a 16% increase compared to that of the devices without PSS-Na. The device with an PSS-Na 0.5mg/mL showed smaller the R_s value and larger the R_p value compared to those of the device without IFL. The performances of PSCs were also dependent on the concentration of PSS-Na solution. The reason for this can be explained as the same case of the PLEDs. The incident photon to collected electron efficiency (IPCE) also demonstrate the photovoltaic parameters are related to the performances of PSCs with PSS-Na treated P3HT:PCBM. The device with PSS-Na shows higher IPCE, with 57.6% at 555 nm as shown in Fig.II-4. This also supports that the device with PSS-Na shows better performances than the device without PSS-Na.

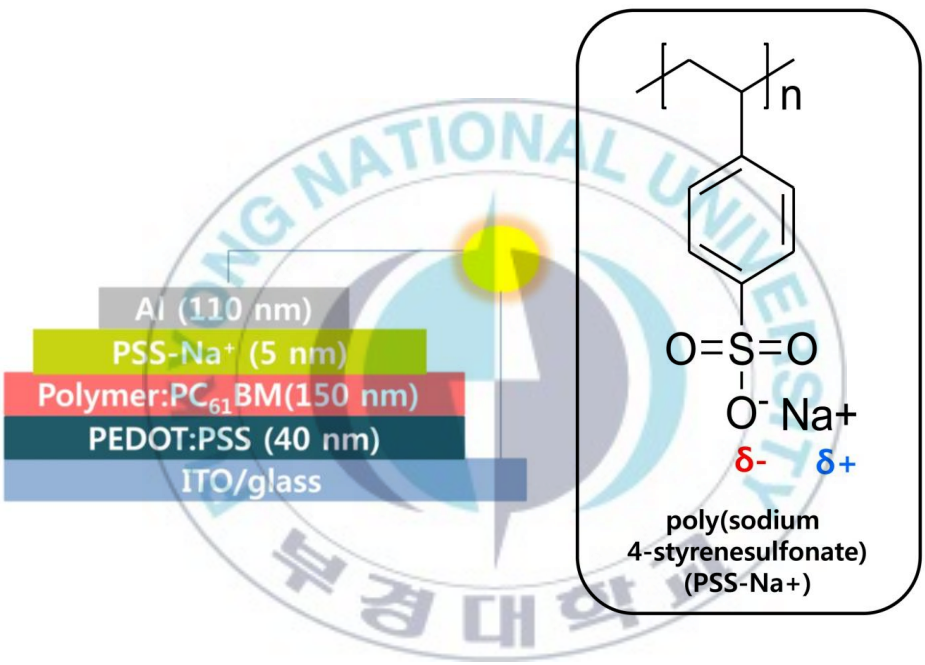

Figure II-2 The structure of PSCs and the chemical structure of PSS-Na

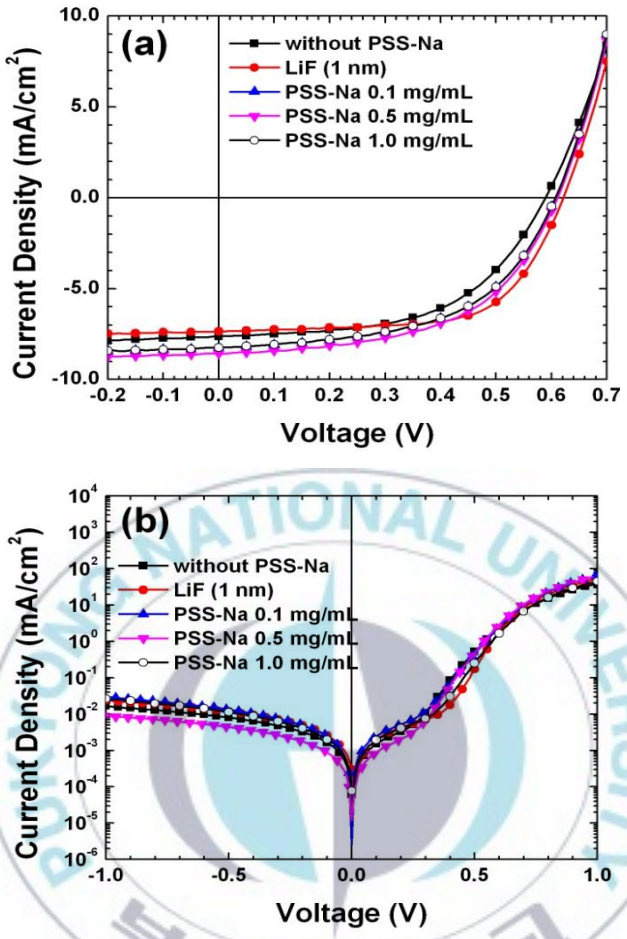

Figure II-3. Current density–voltage curves of PSCs (a) under AM 1.5G simulated illumination with an intensity of 100mW/cm^2 and (b) under the dark condition (filled rectangular: without IFL, filled circle: a 1.0 nm-thick LiF as an IFL, filled triangle: PSS-Na coated from the solution of 0.1 mg/mL, filled reverse triangle: PSS-Na coated from the solution of 0.5 mg/mL, circle: PSS-Na coated from the solution of 1.0 mg/mL).

Table 2-1. The summary of photovoltaic parameters of PSCs with the best PCE value. The averages for photovoltaic parameters of each device are given in parentheses with mean variation.

	V_{oc} (V)	J_{sc} (mA/cm^2)	FF (%)	PCE (%)	R_s (Ωcm^2)[a]	R_p (kΩcm^2)[b]
Without PSS-Na	0.59 (0.59 ± 0.01)	-7.64 (-7.59 ± 0.21)	54.1 (54.5 ± 1.67)	2.44 (2.43 ± 0.95)	5.76	62.8
LiF (1nm)	0.62 (0.62 ± 0.01)	-7.35 (-7.43 ± 0.08)	64.7 (64.1 ± 0.65)	2.95 (2.95 ± 0.03)	2.77	43.0
PSS-Na (0.1 mg/mL)	0.61 (0.61 ± 0.01)	-8.25 (-8.20 ± 0.07)	53.5 (53.8 ± 0.28)	2.69 (2.67 ± 0.03)	2.63	33.9
PSS-Na (0.5 mg/mL)	0.61 (0.61 ± 0.01)	-8.58 (-8.32 ± 0.10)	54.0 (54.69 ± 0.24)	2.83 (2.77 ± 0.07)	3.39	113
PSS-Na (1.0 mg/mL)	0.61 (0.62 ± 0.01)	-7.47 (-7.41 ± 0.10)	54.7 (54.2 ± 0.28)	2.49 (2.47 ± 0.04)	3.48	38.7

[a]: the series resistance (estimated from the device with the best PCE value).

[b]: the parallel resistance (estimated from the device with the best PCE value).

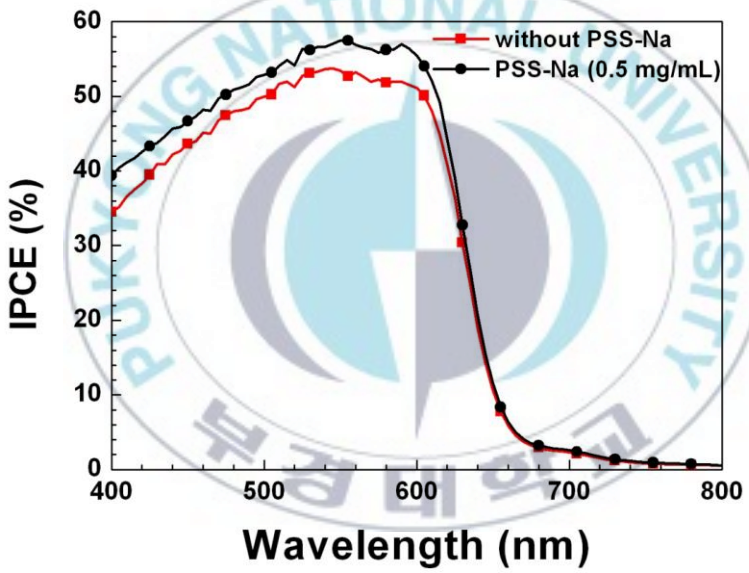

Figure II-4. IPCE Spectra of PSCs without PSS-Na and with PSS-Na

II-3-3. Luminescent properties of PLEDs

To study the properties of PSS-Na when using them as a cathode buffer layer in PLEDs, PLEDs were fabricated with a configuration of ITO/PEDOT/PF9B/PSS-Na/Al (Figure II-5). The Figure II-6, II-7 and Table 2-2 show the characteristic and performances of PLEDs with or without EIL. The device without a buffer layer showed a turn on voltage (V_{on}) (defined by the voltage was required to give a luminescent of 1 cd/m^2) of 5.5 V, a maximum luminance efficiency (LE_{max}) of 0.316 cd/A, a maximum brightness (B_{max}) of 476 cd/m^2 ,respectively. On the contrary, the device with 0.5 mg/mL PSS-Na showed a V_{on} of 5.5 V, a LE_{max} of 3.00 cd/A, a B_{max} of 4348 cd/m^2, respectively. The device with concentration of 0.5 mg/mL PSS-Na is dramatically improved than the device without PSS-Na. And the device with 0.1 mg/mL PSS-Na showed a V_{on} of 7.0 V, a LE_{max} of 0.66 cd/A, a B_{max} of 1436 cd/m^2, and the device with 1.0 mg/mL PSS-Na showed a V_{on} of 7.5 V, a LE_{max} of 2.49 cd/A, a B_{max} of 643 cd/m^2, respectively. The performances of PLEDs were related to the concentration of PSS-Na solution. The performances of the device with 0.1 mg/mL PSS-Na showed very poor performances. One possible reason is that emissive layer is not fully enveloped with the PSS-Na. In case of the device with 1.0 mg/mL PSS-Na, the PSS-Na film was too thick. But the V_{on} values of the devices with the PSS-Na film were smaller than that of the device without PSS-Na, indicating that the electron injecting process is facilitated by the PSS-Na film.

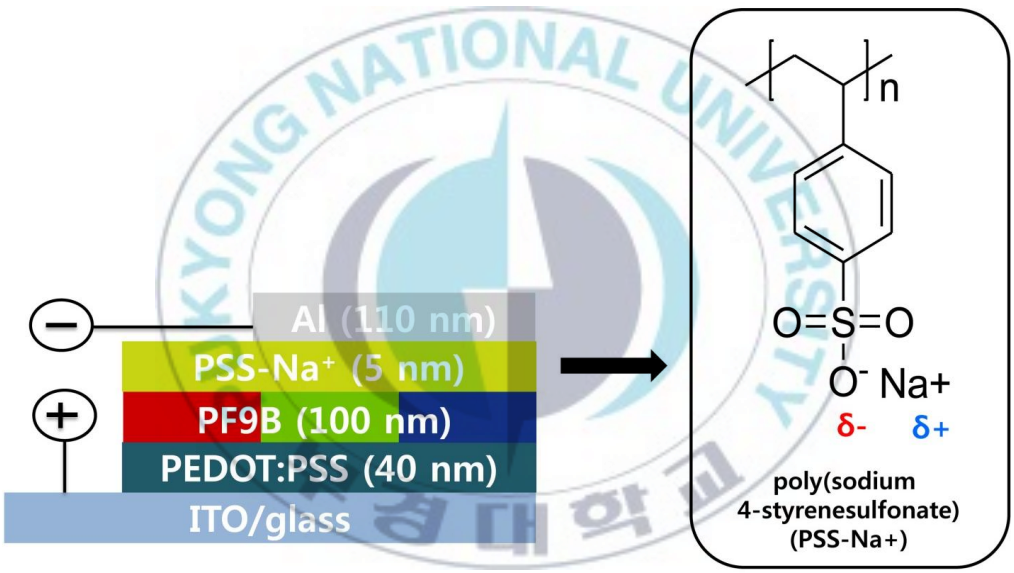

Figure II-5 The structure of PLEDs and The chemical structure of PSS-Na.

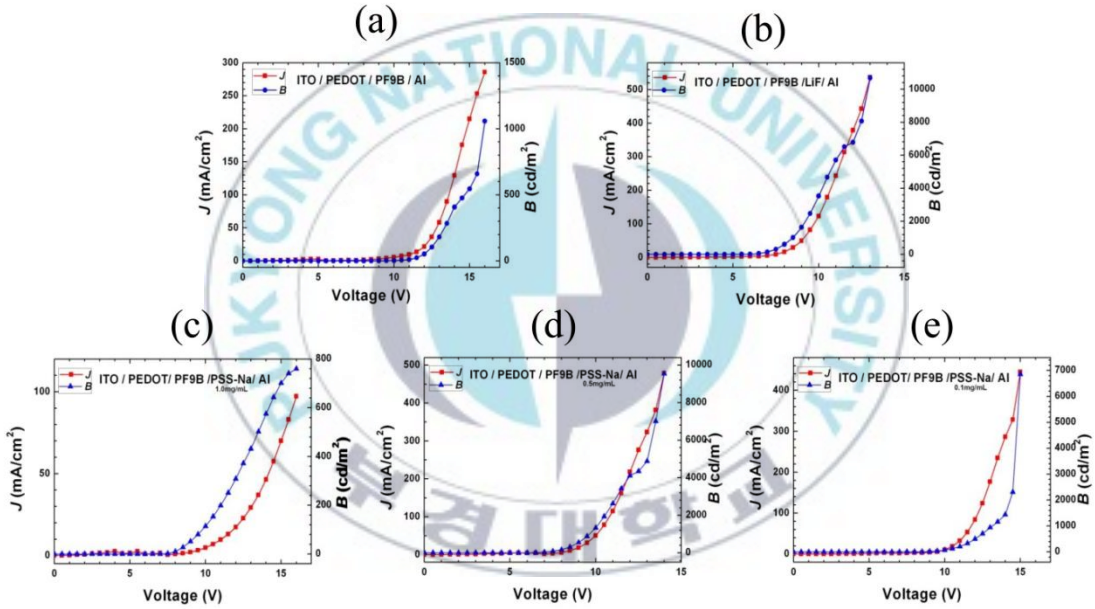

Figure II-6. Current density-voltage-brightness spectra of PLEDs (a) without PSS-Na, (b) with LiF, (c) with PSS-Na of 1.0 mg/mL (d) with PSS-Na of 0.5 mg/mL and (e) with PSS-Na of 0.1 mg/mL.

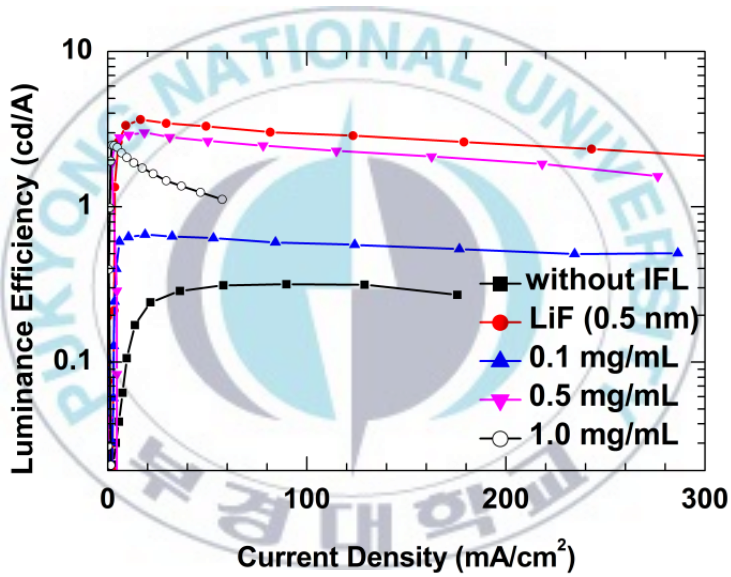

Figure II-7. Luminance efficiency specta of PLEDs without PSS-Na and with PSS-Na.

Table 2-2. The performances of the PLEDs.

	V_{on} [a] (V)	LE_{max} [b] (cd/A) at V	LE_{100} [c] (cd/A)	B_{max} [d] (cd/m^2) at V
Without PSS-Na	9.5	0.316	0.282	476 at 14.5
LiF (0.5 nm)	6.0	3.64	1.97	6518 at 11.5
PSS-Na (0.1 mg/mL)	7.0	0.660	0.649	1436 at 14.0
PSS-Na (0.5 mg/mL)	5.5	3.00	2.56	4348 at 12.5
PSS-Na (1.0 mg/mL)	7.5	2.49	2.47	643 at 14.5

[a] : turn on voltage is defined at a brightness of 1 cd/m^2

[b] : maximum luminance efficiency

[c] : luminance efficiency at a rightness of 100 V cd/m^2

[d] : maximum brightness.

II-3-4. Surface properties of the Active Layer

Figure II-8 shows contact angle images of active layer with or without the thin film of PSS-Na. The static water contact angle of the active layer (P3HT:PCBM) and the PSS-Na coated active layer were (107.9 ± 0.3)° and (99.0 ± 0.2)°, respectively. The PSS-Na coated active layer became more hydrophilic than without PSS-Na. Atomic force microscopy (AFM) images were taken to investigate the morphology of the active layer with or without PSS-Na. The root-mean-square (RMS) roughness of the active layer coated PSS-Na was 2.89 nm. The surface roughness of the PSS-Na coated active layer is more smoother than that of active layer without PSS-Na (3.45 nm). This means that the PSS-Na film can form uniform on the active layer.

\

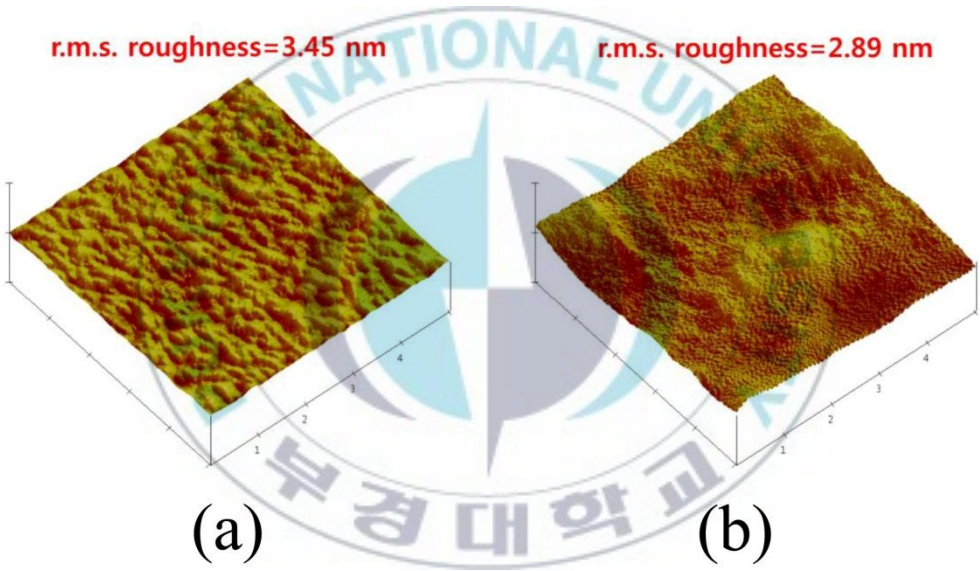

Figure II-8 AFM images of the device (a) without PSS-Na and (b) with PSS-Na

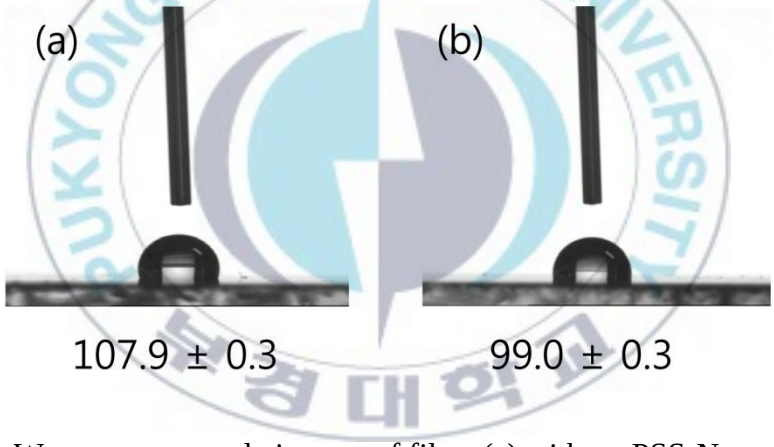

Figure II-9. Water contact angle images of films (a) without PSS-Na and (b) with PSS-Na.

II-4. Conclusion

We have demonstrated an anionic non-conjugated polyelectrolyte, PSS-Na, to modify the property at the organic/Al interface in either PLEDs and PSCs. The UPS and KPM study indicate that Schottky barrier between the organic layer and the Al cathode is reduced by the formation of favorable interface dipole by the PSS-Na film. The performances of PLEDs and PSCs depend in the thickness of the PSS-Na film. The PLED and PSC with the PSS-Na film spin-coated from a solution of 0.5 mg/mL showed best performances, which are higher than those of the device without the PSS-film. This research provides very simple and facile strategy for the enhancement of efficiency of the optoelectronic devices.

References

1. Yu, J. Gao, J. C. Hummelen, F. Wudl, A. J. Heeger, (1995) Science, 270, 1789-1791.

2. Mihee Heo , Heesook Cho , Jae-Woo Jung , Jong-Ryul Jeong , Soojin Park and Jin Young Kim (2011) Adv. Mater. 23, 5689–5693

3. Ma, W. L.; Yang, C. Y.; Gong, X.; Lee, K.; Heeger, A. J. (2005) Adv. Funct. Mater., 15, 1617–1622.

4. I. D. Parker , (1994) J. Appl. Phys., 75 , 1656 .

5. Peet, J.; Kim, J. Y.; Coates, N. E.; Ma, W.; Moses, D.; Heeger, A. J.; Bazan, G. C. (**2007**) *Nat. Mater*., 6, 497–500.

6. Liang, Y. Y.; Wu, Y.; Feng, D.; Tsai, S.-T.; Son, H.-J.; Li, G.; Yu, L. (**2009**) J. Am. Chem. Soc., 131(1), 56–57

7. C. Deibe , T. Strobe , V. Dyakonov , (2010) Adv. Mater. , 22 ,4097 .

8. H. Y. Chen , J. Hou , S. Zhang , Y. Liang , G. Yang , Y. Yang , L. Yu , Y. Wu ,G. Li , (2009) Nat. Photonics , 3 , 649 .

9. Y. Liang , Z. Xu , J. Xia , S. T. Tsai , Y. Wu , G. Li , C. Ray , L. Yu , Adv.Mater. 2010 , 22 , E135 .

10. G. Zhao , Y. He , Y. Li , (2010) Adv. Mater. 22 , 4355 .

11. L. Chen , B. Zhang , Y. Cheng , Z. Xie , L. Wang , X. Jing , F. Wang , (2010) Adv.Funct. Mater. 20 , 3143 .

12. S. C. Price , A. C. Stuart , L. Yang , H. Zhou , W. You , (2011) J. Am. Chem. Soc. 133 , 4625 .

13. Y. Sun , C. J. Takacs , S. R. Cowan , J. H. Seo , X. Gong , A. Roy , A. J. Heeger , (2011) Adv. Mater. 23 , 2226 .

14. T. W. Lee , O. O. Park , (2000) Adv. Mater. 12 , 801 .

15. Y. Shi , J. Liu , Y. Yang , (2000) J. Appl. Phys. 87 , 4254 .

16. J. Jo , S. S. Kim , S. I. Na , B. K. Yu , D. Y. Kim , (2009) Adv. Funct. Mater.19 , 866 .

17. A. J. Moulé , K. Meerholz , (2009) Adv. Funct. Mater. 19 , 3028 .

18. P. W. M. Blom , V. D. Mihailetchi , L. J. A. Koster , D. E. Markov , (2007) Adv.Mater, 19 , 1551 .

19. S. H. Park , A. Roy , S. Beaupré , S. Cho , N. Coates , J. S. Moon ,D. Moses , M. Leclerc , K. Lee , A. J. Heeger , (2009) Nat. Photonics, 3 ,297 .

20. de Jong, M. P.; van Ijzendoorn, L. J.; de Voigt, M. J. A.; (**2000**) Appl. Phys. Lett., **77**, 2255-2257

21. Khodabakhsh, S.; Sanderson, B. M.; Nelson, J.; Jones, T. S. (**2006**) Adv. Funct. Mater. 16, 95-100.

22. Goh, C.; Scully, S. R.; McGehee, M. D. (**2007**) J. Appl. Phys. 101, 114503-114503-12.

23. Kang, H., Hong, S.; Lee, J.; Lee, K. **(2012)** Adv. Mater. 24, 3005–3009.

24. Choi, H.; Park, J. S.; Jeong, E.; Kim, G. -W.; Lee, B. R.; Kim, S. O.; Song, M. H.; Woo, H. Y.; Kim, J. Y.(**2011**) *Adv. Mater*. *23*, 2759–2763.

25. Oh, S. -W.; Na, S. -I.; Jo, J.; Lim, B.; Vak, D.; Kim, D. -Y.(**2010**) *Adv. Funct. Mater*. *20*, 1977-1983.

26. Ma, W.; Iyer, P. K.; Gong, X.; Kiu, B.; Moses, D.; Bazan, G. C.; Heeger, A. J. (**2005**) *Adv. Mater*. 17, 274-277.

27. Na, S.-I.; Oh, S.-H.; Kim, S.-S.; Kim, D.-Y.(**2009**) *Org. Elec*, *10*, 496-500.

28. Choi, H.; Park, J. S.; Jeong, E.; Kim, G. -W.; Lee, B. R.; Kim, S. O.; Song, M. H.; Woo, H. Y.; Kim, J. Y. (**2011**) *Adv. Mater*. *23*, 2759–2763.

29. Oh, S. -W.; Na, S. -I.; Jo, J.; Lim, B.; Vak, D.; Kim, D. -Y. **(2010)** *Adv. Funct. Mater*. *20*, 1977-1983.

30. Ma, W.; Iyer, P. K.; Gong, X.; Kiu, B.; Moses, D.; Bazan, G. C.; Heeger, A. J. (**2005**) *Adv. Mater*. 17, 274-277.

31. Na, S.-I.; Oh, S.-H.; Kim, S.-S.; Kim, D.-Y. (**2009**) *Org. Elec*. *10*, 496-500.

32. Jo, M. Y.; Ha, Y. E.; Kim, J. H. (**2012**) *Sol. Energy Mater. Sol. Cells*, *107*, 1-8.

33. Jo, M. Y.; Ha, Y. E.; Kim, J. H., (2013) *Org. Elec*,14, 995-1001

34. Zhu, X.; Xie, Y.; Li, X.; Qiao, X.; Wang, L.; Tu, G. (**2012**) *J. Mater. Chem.* *22*, 15490-15494.

35. Jin, Y.; Bazan, G. C.; Heeger, A. J.; Kim, J. Y.; Lee, K. (**2008**) Appl. Phys. Lett. 93, 123304 -1 - 123304-3.

36. Heo,M.H ,;Cho,H.S ,; Jung,J.W ,; Jeong,J.R ,; Park,S.J ,; Kim,J.Y (**2011**) Adv. Mater., 23, 5689–5693

37. F. C. Krebs (2008) *Sol. Energy Mater. Sol. Cells*, 92, 7, 715–726,

38. W. Gaynor, J. Y. Lee, and P. Peumans, (2010) ACS Nano, 4, 1, 30–34

39. C. Girotto, B. P. Rand, S. Steudel, J. Genoe, and P. Heremans, (2009) *Org. Elec*, 10, 4, 735–740,

40. S. K. Hau, H. L. Yip, K. Leong, and A. K. Y. Jen, (2009) *Org. Elec*,10,719–723

41. M. S. White, D. C. Olson, S. E. Shaheen, N. Kopidakis, and D. S. Ginley, (2006) *Appl. Phys. Lett.*, 89, 14, 143517

42. S. K. Hau, H.-L. Yip, H. Ma, and A. K.-Y. Jen, (2008) *Appl. Phys. Lett.*, 93, 23, 233304,

43. Waldauf, M. Morana, P. Denk et al., (2006) *Appl. Phys. Lett.*, 89, 23, 233517,

44. R. Steim, S. A. Choulis, P. Schilinsky, and C. J. Brabec, (2008) *Appl. Phys. Lett.*, 92,. 9, 093303,

45. S. K. Hau, H. L. Yip, O. Acton, N. S. Baek, H. Ma, and A. K. Y. Jen, (2008) J. Mater. Chem, 18,. 42, 5113–5119,

46. Zhiwen Zheng,a Qingchen Dong,b Liao Gou,a Jian-Hua Su*a and Jinhai Huang (2014) J. Mater. Chem. C, 2, 9858–9865

47. Norbert Koch, (2007) Chem Phys Chem , 8, 1438 – 1455

48. Martine Wolf and Hans Rauschenbacht (1963) Advanced Energy Conversion. 3, 455-479.

49. Boyuan Qiab and Jizheng Wang (2013) Phys. Chem. Chem. Phys., 15, 8972—8982

50. Jonathan D. Servaites, Mark A. Ratner and Tobin J. Marks (2011) Energy Environ. Sci., 2011, 4, 4410

51. J. Cabestany and L. Castañer (1983) Revue Phys. Appl. 18, 565-567

52. Antonio Guerrero, Teresa Ripolles-Sanchis, Pablo P. Boix, Germa Garcia-Belmonte (2012) *Org. Elec*, 13, 2326–2332

53. Bernard Geffroy, Philippe le Roy and Christophe Prat (2006) Polym Int, 0959–8103

54. Roland Steim,*F. Ren_e Koglera and Christoph J. Brabec (2010) J. Mater. Chem.10, 20, 2499–2512

55. Slawomir Braun, William R. Salaneck, and Mats Fahlman (2009) Adv. Mater. 21, 1450–1472

56. W. Hu, Y. Zhao, J. Hou, C. Ma, and S. Liu, (2007) Microelectronics J, 38, 632-636

57. C. J. Brabec, S. E. Shaheen, C. Winder, N. S. Sariciftci, and P. Denk, (2002) *Appl. Phys. Lett.*, 80,1288

58. T. M. Brown, R. H. Friend, I. S. Millard, D. J. Lacey, J. H. Burroughes, and F. Cacialli, (2000) *Appl. Phys. Lett.*, vol. 77, 3096

59. E. Nam, S. Oh, D. Jung, H. Kim, H. Chae, and J. Yi, (2012) *Semicond. Sci. Technol.*, 27, 105004

60. Takayuki Kuwabara *, Hirokazu Sugiyama, Mitsuhiro Kuzuba, Takahiro Yamaguchi, Kohshin Takahashi (2010) *Org. Elec* 11, 1136–1140

61. Kwanghee Lee, Jin Young Kim, Sung Heum Park, Sun Hee Kim, Shinuk Cho, and Alan J. Heeger (2007) Adv. Mater. 19, 2445–2449

62. Jin Young Kim, Sun Hee Kim, Hyun-Ho Lee, Kwanghee Lee, Wanli Ma, Xiong Gong, and Alan J. Heeger (2006) Adv. Mater. 18, 572–576

63. Chuen-Shii Chou, Chuen-Shyong Chou, Yi-Ting Kuo , Chun-Po Wang (2013) Adv.Powder.Technol, 24, 336–343

64. Tae Hwan Lima, Kyung Wha Oh, Seong Hun Kim (2012) *Synt. Met.* 162, 268– 275

65. Zhu, X.; Xie, Y.; Li, X.; Qiao, X.; Wang, L.; Tu, G. (2012) *J. Mater. Chem. 22*, 15490-15494.

66. Jin, Y.; Bazan, G. C.; Heeger, A. J.; Kim, J. Y.; Lee, K. (2008) *Appl. Phys. Lett. 93*, 123304 -1 - 123304-3.

67. Mihee Heo , Heesook Cho , Jae-Woo Jung , Jong-Ryul Jeong , Soojin Park , and Jin Young Kim (2011) Adv. Mater. 23, 5689–5693

68. Ye Eun H,Gyeong Eun Lim,Mi Young Jo,Juyun Park,Yong-Cheol Kang,Sang-Jin Moon and Joo Hyun Kim (2014) *J. Mater. Chem. C*, 2, 3820-3825

69. Herguth, P.; Jiang, X.; Liu, M. S.; Jen, A. K. –Y. (2002) *Macromolecules*, *35*, 6094-6100.

70. Ishii, H.; Sugiyama, K.; Ito, E.; Seki, K. (1999) *Adv. Mater*, *11* , 605-625.